T-bet-dependent NKp46^{+} innate lymphoid cells regulate the onset of T_H17-induced neuroinflammation

Brandon Kwong[1,6], **Rejane Rua**[2,6], **Yuanyuan Gao**[1], **John Flickinger Jr.**[1], **Yan Wang**[1], **Michael J. Kruhlak**[1], **Jinfang Zhu**[3], **Eric Vivier**[4,5], **Dorian B. McGavern**[2], and **Vanja Lazarevic**[1]

[1]Experimental Immunology Branch, National Cancer Institute, National Institutes of Health, Bethesda, Maryland, USA

[2]Viral Immunology and Intravital Imaging Section, National Institute of Neurological Disorders and Stroke, National Institutes of Health, Bethesda, Maryland, USA

[3]Laboratory of Immunology, National Institute of Allergy and Infectious Diseases, National Institutes of Health, Bethesda, Maryland, USA

[4]Aix Marseille Univ, CNRS, INSERM, CIML, Marseille, France

[5]AP-HM Hôpital de la Timone, Serce d'Immunologie, Marseille, France

Abstract

The transcription factor T-bet has been linked to increased susceptibility to systemic and organ-specific autoimmunity, but the mechanism by which T-bet expression promotes neuroinflammation remains unknown. In this study, we demonstrate a cardinal role for T-bet-dependent NKp46^{+} innate lymphoid cells (ILCs) in the initiation of CD4^{+} T_H17-mediated neuroinflammation. Loss of T-bet specifically in NKp46^{+} ILCs profoundly impaired the ability of myelin-reactive T_H17 cells to invade the central nervous system (CNS) tissue and protected the mice from autoimmunity. T-bet-dependent NKp46^{+} ILCs were localized in the meninges and acted as chief coordinators of meningeal inflammation by inducing the expression of pro-inflammatory cytokines, chemokines and matrix metalloproteinases, which in a concerted fashion facilitated T cell entry into CNS parenchyma. Our findings uncover a detrimental role of T-bet-dependent NKp46^{+} ILCs in the development of CNS autoimmune disease.

Correspondence should be addressed to V.L. (lazarevicv@mail.nih.gov).
[6]Equal contribution

AUTHOR CONTRIBUTIONS

B.K. conducted the experiments, analyzed the data and contributed to the first draft of the manuscript preparation. R.R., Y.Y.G., J.F., Y.W. conducted experiments and analyzed the data. D.B.M. contributed to the experimental design and manuscript preparation. M.J.K. performed quantitation of apoptotic cells in the CNS in a blinded manner. E.V. and J.Z. generated NKp46-Cre^{+} and T-bet ZsGreen reporter mice, respectively. V.L. designed and directed the study, conducted the experiments, analyzed the data and wrote the manuscript.

COMPETING FINANCIAL INTERESTS

The authors declare no competing financial interests.

INTRODUCTION

Multiple sclerosis (MS) is the most common demyelinating disease of the central nervous system and a leading cause of neurological disability in young adults[1]. Considerable progress has been made in our understanding of immunological events that lead to the development of MS using the experimental autoimmune encephalomyelitis (EAE) model of inflammatory demyelination. Genetic targeting of interleukin 12 (IL-12) and IL-23 cytokines, necessary for the development and terminal differentiation of interferon-γ (IFN-γ)–producing $CD4^+$ T helper 1 (T_H1) and IL-17–producing T helper 17 (T_H17) cells, respectively, revealed that T_H17 cells, and not T_H1 cells, are essential for the development of EAE[2–5]. Following peripheral activation, pathogenic T_H17 cells migrate to the CNS and accumulate in the perivascular spaces and meninges. Here, autoantigen-driven T cell reactivation by CNS-resident antigen-presenting cells (APCs) is a prerequisite for the initiation of the inflammatory cascade by T_H17 cells[6]. However, the underlying immunological factors that promote the migration of immune cells from the site of reactivation into CNS parenchyma are still not well understood.

The T-box transcription factor T-bet is critical for the development of immunopathology during EAE[7, 8]. T-bet is encoded by *Tbx21* and is expressed in multiple immune cell lineages of the immune system[9]. As a critical regulator of the type 1 inflammatory response, T-bet is required for the activation of host immune-defense mechanisms against infectious microorganisms[10]. However, excessive T-bet-regulated immune responses have been linked to the pathogenesis of immune-mediated disorders[10]. Although initially defined as the master regulator of the T_H1 differentiation program, accumulating data indicate that T-bet is essential for the pathogenicity of T_H17 cells in EAE[11–13]. Its expression in T_H17 cells is induced in response to IL-12 or IL-23 signaling[11, 12, 14]. T-bet promotes the functional plasticity and amplifies the inflammatory potential of T_H17 cells by upregulating endogenous TGF-β3 production[11, 12]. Whether T-bet expression in immune cells other than T_H17 cells contributes to the pathogenesis of EAE is presently unknown.

Here, we demonstrate that T-bet expression in myelin-reactive T_H17 cells was necessary but not sufficient for the development of EAE. We establish a highly selective requirement for T-bet-dependent $NKp46^+$ ILCs in the initiation of T_H17-mediated neuroinflammation. Specifically, we found that T-bet-dependent $NKp46^+$ ILCs controlled the CNS parenchymal infiltration of myelin-reactive T_H17 cells by generating pro-inflammatory cytokine environment in the meninges that was necessary for the reactivation and maintenance of IL-17A-producing $CD4^+$ T cells in the CNS. Our findings demonstrate a pathogenic role of $NKp46^+$ ILCs in neuroinflammation and identify $NKp46^+$ ILCs as a potential target for the treatment of inflammatory CNS disorders.

RESULTS

T-bet expression in T cells is insufficient to cause EAE

To better understand the role of T-bet in the pathogenesis of autoimmune diseases, we first wanted to determine whether T-bet expression in cells of hematopoietic origin is required for the development of organ-specific immunopathology. To address this question, we generated

conditional T-bet-deficient mice in which *Tbx21* was deleted in hematopoietic cells (*Tbx21*$^{f/f}$ Vav1-Cre^{+} mice). We tested the effects of hematopoietic system-specific deletion of T-bet on susceptibility to EAE by immunizing *Tbx21*$^{f/f}$ Vav1-Cre^{+} mice and their *Tbx21*$^{f/f}$ controls with a CNS-derived antigen, myelin oligodendrocyte glycoprotein peptide amino acids 35–55 (MOG_{35-55}). Hematopoietic ablation of *Tbx21* gene expression resulted in significantly attenuated EAE, phenocopying germline T-bet deficiency (*Tbx21*$^{-/-}$), suggesting that the pathogenic role of T-bet mapped to the cells of the hematopoietic system (Fig. 1a,b).

We therefore sought to determine in which immune cell lineage(s) T-bet expression is required to drive neuroinflammation. To this end, MOG_{35-55} peptide-reactive T-bet-deficient (2D2 *Tbx21*$^{-/-}$) and T-bet-sufficient (2D2 wild-type) CD4^{+} T cells were activated under T_H17-polarizing conditions and adoptively transferred into either T-bet-deficient (*Tbx21*$^{-/-}$) or wild-type hosts. 2D2 *Tbx21*$^{-/-}$ T_H17 cells failed to induce EAE in either *Tbx21*$^{-/-}$ or wild-type recipients (Fig. 1c), confirming the requirement for T-cell-intrinsic expression of T-bet in the pathology of EAE. 2D2 wild-type T_H17 cells, while fully capable of inducing disease in wild-type recipients, were not pathogenic in *Tbx21*$^{-/-}$ recipients, demonstrating that T-cell-intrinsic expression of T-bet cells is necessary, but not sufficient, to cause EAE (Fig. 1c). Furthermore, infiltration of cells into the CNS parenchyma was severely reduced in *Tbx21*$^{-/-}$ recipients compared with wild-type controls (Fig. 1d), which was confirmed by histological analysis (Fig. 1e). These results revealed that T-bet expression in immune cells other than myelin-reactive CD4^{+} T_H17 cells is additionally required for the pathogenesis of autoimmune CNS disease.

Peripheral licensing of CD4^{+} T_H17 cells in *Tbx21*$^{-/-}$ host

Adoptively transferred myelin-reactive CD4^{+} T cells acquire the capacity to enter the CNS after effective activation within the lungs[15]. We asked whether peripheral licensing of adoptively transferred 2D2 wild-type T_H17 cells occurred normally in the lungs of *Tbx21*$^{-/-}$ recipients. We found that adoptively transferred 2D2 wild-type T_H17 cells egressed and proliferated normally in the spleen and lungs of both *Tbx21*$^{-/-}$ and wild-type recipients (Fig. 2a,b). Consistent with previous reports[15, 16], myelin-reactive CD4^{+} T cells transitioned to a migratory mode in the lung by upregulating the expression of integrins α_4 (VLA-4 subunit) and α_L (LFA-1 subunit) and the chemokine receptors CXCR4 and CCR6. Notably, the expression of these adhesion molecules and chemokine receptors on 2D2 wild-type T_H17 cells was not affected by T-bet deficiency in the recipient mice (Fig. 2c). Furthermore, 2D2 CD4^{+} T cells isolated from the spleens and lungs of *Tbx21*$^{-/-}$ and wild-type recipients had similar percentages of cytokine-producing cells (Fig. 2d). Collectively, these data demonstrate that T-bet is not required for the licensing of 2D2 wild-type T_H17 cells in the periphery.

We next sought to determine whether T-bet deficiency in recipient mice affected the effector function of 2D2 wild-type T_H17 in the CNS. In addition to recovering fewer 2D2 CD4^{+} T cells (Fig. 1c), we detected a severe reduction in the frequency of IL-17A^{+}IFN-γ^{-} and IL-17A^{+}IFN-γ^{+} 2D2 CD4^{+} T cells in the CNS of *Tbx21*$^{-/-}$ recipients compared with wild-type controls (Fig. 2e). The adoptive transfer experiments with T-bet-sufficient 2D2 T_H17

cells demonstrate that T-bet expression in a non-T-cell compartment controls the parenchymal infiltration and the effector function of autoreactive $CD4^+$ T_H17 cells in the CNS.

T-bet-expressing cells in the CNS during EAE

We next aimed to identify T-bet-expressing cells that are necessary for the optimal activation of $CD4^+$ T_H17 cells in the CNS during EAE using a previously established T-bet-ZsGreen reporter mouse[17]. Following EAE induction, numerous $ZsGreen^+$ cells could be detected in the meninges, the central canal and throughout the spinal cord parenchyma (Fig. 3a). Approximately 50% of CNS-infiltrating $CD45^+$ leukocytes expressed T-bet at the peak of disease (Fig. 3b). We identified that most T cells, $NK1.1^+$ cells and a fraction of DCs expressed T-bet during EAE (Fig. 3c). The numbers of T-bet-expressing T cells and DCs increased in the CNS from the onset to the peak of disease. In contrast, T-bet-expressing $NK1.1^+$ cells were detected in the CNS at the early stage of disease and their numbers remained unchanged throughout the course of disease (Fig. 3d). Therefore, we proceeded to investigate the impact of T-bet deficiency in T cells, DCs and $NK1.1^+$ cells on the effector function of 2D2 wild-type T_H17 cells and their ability to induce neuropathology.

Endogenous T-bet$^+$ T cells and DCs had no impact on EAE

Analysis of cell infiltration during EAE revealed that the majority of CNS-infiltrating $CD4^+$ T cells were adoptively transferred 2D2 $CD4^+$ T cells, expressing the transgenic T cell receptor chain $V_\beta11$, while approximately 15% of CNS-infiltrating $CD4^+$ T cells were endogenous (host-derived) $CD4^+$ T cells (Supplementary Fig. 1a). To determine whether T-bet expression in endogenous T cells affected the encephalitogenicity of adoptively transferred 2D2 wild-type T_H17 cells, we transferred 2D2 wild-type T_H17 cells into *Tbx21*$^{f/f}$ CD4-Cre^+ recipients, which lack T-bet expression in T cells and natural killer T (NKT) cells, and their littermate *Tbx21*$^{f/f}$ controls. Both endogenous $CD4^+$ T cells and the transferred 2D2 ($V_\beta11^+$) wild-type T_H17 cells migrated efficiently into the CNS of *Tbx21*$^{f/f}$ or *Tbx21*$^{f/f}$ CD4-Cre^+ mice (Supplementary Fig. 1a). In contrast to *Tbx21*$^{f/f}$ controls, endogenous $CD4^+$ T cells in the CNS of *Tbx21*$^{f/f}$ CD4-Cre^+ contained a higher percentage of IL-$17A^+$IFN-γ^- and a significantly lower percentage of IL-$17A^-$IFN-γ^+ cells (Supplementary Fig. 1b); nevertheless, this alteration in the cytokine profile of endogenous $CD4^+$ T cells had no impact on the cytokine production or pathogenicity of adoptively transferred 2D2 wild-type T_H17 cells (Supplementary Fig. 1c,d).

Major histocompatibility complex class II (MHCII)-restricted antigen presentation by meningeal and perivascular $CD11c^+$ DCs and macrophages is required for the reactivation of primed myelin-reactive T cells leading to CNS invasion and clinical disease development[6, 18–20]. Since 2D2 wild-type T_H17 cells showed suboptimal cytokine production in the CNS of *Tbx21*$^{-/-}$ mice, we tested the importance of T-bet expression in DCs by transferring 2D2 wild-type T_H17 cells into *Tbx21*$^{f/f}$ CD11c-Cre^+ recipients, which lack T-bet expression in DCs, and their *Tbx21*$^{f/f}$ controls. We found that DC-specific loss of T-bet had no effect on the pathogenicity of adoptively transferred 2D2 wild-type T_H17 cells in the CNS (Supplementary Fig. 2a,b). Collectively, these results show that the infiltration and optimal effector function of adoptively transferred 2D2 wild-type T_H17 cells in the CNS

is not dependent on T-bet expression in endogenous (host-derived) T cells, NKT cells and DCs.

T-bet-dependent NKp46^{+} ILCs initiate T_H17-mediated EAE

To ascertain the relevance of NK1.1^{+} cells in T_H17-induced neuroinflammation, we depleted NK1.1^{+} cells in *Tbx21*$^{-/-}$ and wild-type hosts via intravenous injections of the anti-NK1.1 depleting antibody before the adoptive transfer of 2D2 wild-type T_H17 cells and repeatedly during EAE (Supplementary Fig. 3). *Tbx21*$^{-/-}$ recipients depleted of NK1.1^{+} cells remained resistant to EAE induction by 2D2 wild-type T_H17 cells (Fig. 4a). By contrast, wild-type mice treated with anti-NK1.1 showed significantly attenuated EAE disease course compared to controls (Fig. 4b), suggesting that NK1.1^{+} cells have a pathogenic role in T_H17-driven neuropathology.

T-bet is a key factor in the terminal maturation and homeostasis of NK and $V_{\alpha}14i$ NKT cells and in lineage specification of ILC1 and the NKp46^{+} ILC3[21–27]. To evaluate the requirement for T-bet in NK cells, ILC1 and the NKp46^{+} subset of ILC3, we generated mice harboring genetic deletion of T-bet in all three ILC subsets by crossing *Tbx21*$^{f/f}$ mice to NKp46-Cre^{+} (also known as Ncr1-Cre^{+}) transgenic mice. Following the adoptive transfer of 2D2 wild-type T_H17 cells, mice with the NKp46-specific ablation of T-bet (*Tbx21*$^{f/f}$ NKp46-Cre^{+}) exhibited significantly reduced mean clinical scores and percent disease incidence compared to controls (Fig. 4c,d). However, the maximum EAE disease score among symptomatic *Tbx21*$^{f/f}$ NKp46-Cre^{+} mice was not significantly different from *Tbx21*$^{f/f}$ controls (Fig. 4d). These results demonstrate that the primary function of T-bet-dependent NKp46^{+} ILCs is to control the onset of T_H17-mediated neuroinflammation, but once the disease is induced, they are not required for the effector stage of neuroinflammation.

Localization of T-bet-dependent NKp46^{+} ILCs during EAE

The meninges of the CNS constitute an additional licensing checkpoint where autoantigen-driven T cell reactivation by CNS-resident APCs is a prerequisite for CNS parenchymal infiltration and subsequent demyelinating pathology[6]. Since T-bet-dependent NKp46^{+} ILCs affected the onset of T_H17-mediated neuroinflammation, we hypothesized that the NKp46^{+} ILCs were strategically positioned in the meninges where they mediate the process of 2D2 wild-type T_H17 cell reactivation. To assess this possibility, we have utilized a combination of high-resolution confocal microscopy and histo-cytometry to directly investigate the localization of NKp46^{+} ILCs, 2D2 CD4^{+} T_H17 cells and MHCII-expressing APCs (Fig. 5a,b). The most prominent feature of the immune response in the meninges was the formation of discrete cellular clusters containing large numbers of NKp46^{+} ILCs tightly juxtaposed to both MHCII^{+} APCs and 2D2 CD4^{+} T cells. The NKp46^{+} ILC–T cell–APC clusters could be detected in the spinal cord meninges even before the onset of symptoms (score 0, Fig. 5a), indicating that they may designate the precise anatomical location of 2D2 CD4^{+} T cells reactivation. Preferential localization of NKp46^{+} ILCs within the dense clusters of MHCII^{+} APCs and 2D2 CD4^{+} T cells was additionally confirmed by histo-cytometry (Fig. 5b, blue boxes). Collectively, these observations demonstrate that NKp46^{+} ILC are localized in the meninges where they could foster 2D2 CD4^{+} T cell reactivation by influencing the function of APCs and/or autoreactive CD4^{+} T cells.

Pathogenic function of T-bet maps to ILC1/NKp46$^+$ ILC3

To investigate the significance of NKp46$^+$ ILCs in the pathophysiology of CD4$^+$ T_H17-mediated neuroinflammation, we used multi-parameter flow cytometry to identify ILCs subsets and analyze their function in the meninges of *Tbx21*$^{f/f}$ and *Tbx21*$^{f/f}$ NKp46-Cre$^+$ recipients. In comparison to control mice, the meninges of *Tbx21*$^{f/f}$ NKp46-Cre$^+$ mice exhibited a profound deficiency in NKp46$^+$ ILCs (Fig. 6a,b). We observed a significant reduction in the numbers of conventional NK cells and ILC1s while the number of NKp46$^+$ ILC3s was comparable between *Tbx21*$^{f/f}$ and *Tbx21*$^{f/f}$ NKp46-Cre$^+$ recipients (Fig. 6c). T-bet-dependent NKp46$^+$ ILCs predominantly produced IFN-γ and very few IFN-γ-producing NK cells and ILC1 were detected in the meninges of *Tbx21*$^{f/f}$ NKp46-Cre$^+$ mice (Fig. 6a,c). Additionally, a twofold reduction in the number of IFN-γ-producing NKp46$^+$ ILC3s was detected in the meninges of *Tbx21*$^{f/f}$ NKp46-Cre$^+$ mice (Fig. 6c). Collectively, these results demonstrate that a selective loss of T-bet in NKp46$^+$ ILCs resulted in meningeal depletion of NK cells and ILC1 and reduced IFN-γ-production by NKp46$^+$ ILC3s.

NK cells are the numerically dominant population of T-bet-dependent NK1.1$^+$ NKp46$^+$ ILCs. However, the role of NK cells in EAE has been controversial. Several studies have shown that NK cells can have either pathogenic or protective functions in EAE[28–32]. To clarify this long-standing issue of the relevance of NK cells in EAE, we have generated NK cell-deficient *Eomes*$^{f/f}$ NKp46-Cre$^+$ mice (Supplementary Fig. 4a,b)[33]. Passive transfer of 2D2 wild-type T_H17 cells induced EAE of equal severity in NK cell-sufficient and NK cell-deficient mice (Fig. 6d,e), demonstrating that NK cells do not have a leading role in T_H17-induced neuroinflammation. Therefore, the pathogenic role of T-bet within NKp46$^+$ ILCs maps to ILC1 and/or the NKp46$^+$ subset of ILC3.

NKp46$^+$ ILCs regulate infiltration of CD4$^+$ T_H17 cells

Under pathological conditions, meningeal and parenchymal infiltration of immune cells is heavily influenced by the inflammatory environment in the meninges[34]. ILCs are a potent innate cellular source of pro-inflammatory cytokines. To test the contribution of T-bet-dependent NKp46$^+$ ILCs to meningeal inflammation, we isolated the meninges from naïve mice and *Tbx21*$^{f/f}$ and *Tbx21*$^{f/f}$ NKp46-Cre$^+$ mice, previously injected with 2D2 wild-type T_H17 cells, and measured the expression of transcripts encoding pro-inflammatory cytokines by quantitative RT-PCR. Compared to naive mice, transcripts encoding pro-inflammatory cytokines such as *p40*, *p35*, *p19*, *Il1b*, *Il6*, *Tnf*, *Lta*, *Il17a* and *Ifng* were upregulated in the meninges of *Tbx21*$^{f/f}$ mice (Fig. 7a). By contrast, loss of T-bet expression in NKp46$^+$ ILCs resulted in significantly decreased expression of *p35*, *p19*, *Il1b*, *Il6*, *Tnf*, *Lta*, *Il17a* and *Ifng*, demonstrating that T-bet-dependent NKp46$^+$ ILCs shape, directly or indirectly, inflammatory microenvironment in the meninges during T_H17-mediated neuroinflammation (Fig. 7a). We hypothesized that ILC-mediated cytokine changes in the meninges, may be an important factor controlling parenchymal infiltration of immune cells. We found that meningeal accumulation of 2D2 wild-type T_H17 cells was not significantly different between *Tbx21*$^{f/f}$ and *Tbx21*$^{f/f}$ NKp46-Cre$^+$ mice. In contrast, parenchymal infiltration of 2D2 wild-type T_H17 cells was significantly reduced in *Tbx21*$^{f/f}$ NKp46-Cre$^+$ mice (Fig. 7b), which was confirmed by histological analysis (Fig. 7c). Integrins α_4 and α_L are required for the firm adhesion and extravasation of encephalitogenic T cells while CCR6 and its ligand

CCL20 regulate the entry of T_H17 cells into the CNS[35–37]. We found that the CNS-infiltrating 2D2 $CD4^+$ T cells expressed comparable amounts of both integrins and CCR6 in *Tbx21*$^{f/f}$ and *Tbx21*$^{f/f}$ NKp46-Cre^+ mice (Fig. 7d), indicating that the lack of migration into CNS parenchyma is not due to a T cell-intrinsic defect and that meningeal T-bet-dependent $NKp46^+$ ILCs may regulate the parenchymal infiltration of 2D2 $CD4^+$ T cells.

T-bet-dependent $NKp46^+$ ILCs could affect 2D2 $CD4^+$ T_H17 cell parenchymal infiltration indirectly by influencing the capacity of meningeal APCs to reactivate 2D2 $CD4^+$ T_H17 cells *in situ*. Activation of APCs, as measured by upregulation of MHCII, CD80 and ICAM-1, is dependent on IFN-γ. Like *Tbx21*$^{f/f}$ NKp46-Cre^+ mice, *Ifng*$^{-/-}$ recipient mice were protected from T_H17-mediated neuroinflammation in the passive EAE model (Supplementary Fig. 5a)[38]. *Ifng*$^{-/-}$ mice showed a significant defect in the recruitment of 2D2 $CD4^+$ T cells, myeloid DCs (mDCs), inflammatory monocytes (iMO) and neutrophils to the spinal cord meninges following the adoptive transfer of 2D2 wild-type T_H17 cells (Supplementary Fig. 5b,c). Additionally, resident APCs ($CD206^+$ perivascular macrophages, PVMs) failed to upregulate MHCII, CD80 and ICAM1 while mDCs showed significantly reduced expression of CD80 and ICAM1 in the meninges of *Ifng*$^{-/-}$ mice (Supplementary Fig. 5d and Supplementary Fig. 6 for gating strategy). Collectively, these data establish that IFN-γ is of a critical importance in driving the recruitment and activation of meningeal APCs. Next, we asked whether IFN-γ expression by $NKp46^+$ ILCs was essential for optimal activation of meningeal APCs and, consequently, for optimal reactivation of 2D2 $CD4^+$ T cells *in vivo*. In contrast to *Ifng*$^{-/-}$ mice, *Tbx21*$^{f/f}$ NKp46-Cre^+ mice showed normal recruitment and activation of meningeal APCs following the adoptive transfer of 2D2 wild-type T_H17 cells (Supplementary Fig. 7a,b), demonstrating that the expression of IFN-γ by $NKp46^+$ ILCs is not required for the recruitment or activation of meningeal APCs, and that other cellular sources of IFN-γ could compensate for the lack of innate source of IFN-γ.

Under neuroinflammatory conditions, the gradient of chemokines produced and induced by meningeal immune cells promotes leukocyte transmigration across the blood brain barrier (BBB) into the CNS parenchyma[39]. The expression of matrix metalloproteinases (MMPs) by both resident and immune cells strongly enhances this transmigration process by breaking down the glia limitans as well as by modulating the activity of chemokines at the parenchymal border[40]. Since the expression of MMPs and chemokines is regulated by proinflammatory cytokines, we hypothesized that T-bet-dependent $NKp46^+$ ILCs facilitated 2D2 $CD4^+$ T_H17 cell parenchymal infiltration indirectly by inducing the expression of MMPs and chemokines in the meninges and parenchyma, respectively. To test this hypothesis, we examined MMP and chemokine expression in the meninges and parenchyma of *Tbx21*$^{f/f}$ and *Tbx21*$^{f/f}$ NKp46-Cre^+ mice following adoptive transfer of 2D2 wild-type T_H17 cells by quantitative RT-PCR. Loss of T-bet expression in $NKp46^+$ ILCs abrogated the expression of major MMPs implicated in EAE such as *Mmp2*, *Mmp3*, *Mmp9*, *Mmp13*, *Mmp14* and *Mmp19* in the meninges (Fig. 7e). Additionally, significantly fewer chemokine mRNAs (*Ccl2*, *Ccl3*, *Ccl4, Ccl5, Ccl20*, *Cxcl9, Cxcl1)* were measured in the parenchyma of *Tbx21*$^{f/f}$ NKp46-Cre^+ mice compared to *Tbx21*$^{f/f}$ controls (Fig. 7f), indicating that optimal chemokine gradient was not established in the parenchyma of *Tbx21*$^{f/f}$ NKp46-Cre^+ mice. Although transferred 2D2 wild-type T_H17 cells expressed comparable amounts of CCR6 (Fig. 7d), diminished parenchymal expression of *Ccl20* (CCR6 ligand) could account for the

migratory defect of T_H17 cells into the CNS parenchyma of *Tbx21*$^{f/f}$ NKp46-Cre$^+$ mice. These data demonstrate that T-bet-dependent NKp46$^+$ ILCs induce the expression of MMPs and chemokines which disrupt the BBB and guide the migration of 2D2 CD4$^+$ T cells out of meninges into the CNS parenchyma, respectively.

NKp46$^+$ ILCs regulate the stability of CD4$^+$ T_H17 cells

Functional stability and pathogenicity of CD4$^+$ T_H17 cells is dependent on the APC-derived cytokines IL-1β, IL-6, IL-23, TNF-α and LT-α[3, 4, 14, 41–43]. Since the expression of aforementioned cytokines was significantly reduced in the meninges of *Tbx21*$^{f/f}$ NKp46-Cre$^+$ mice, we next investigated whether the maintenance of T_H17 responses was affected in the CNS of *Tbx21*$^{f/f}$ NKp46-Cre$^+$ mice. We observed a decrease in the frequency of IL-17A$^+$IFN-γ$^-$ and an increase in the frequency of IL-17A$^-$IFN-γ$^+$ 2D2 CD4$^+$ T cells both in the meninges and parenchyma of *Tbx21*$^{f/f}$ NKp46-Cre$^+$ recipients compared to *Tbx21*$^{f/f}$ controls (Fig. 8a,b). We additionally detected significantly less of *Il17a* transcripts in total CNS extracts of *Tbx21*$^{f/f}$ NKp46-Cre$^+$ mice compared with *Tbx21*$^{f/f}$ controls confirming diminished IL-17A production (Fig. 8c). These data demonstrate that the loss of T-bet expression in NKp46$^+$ ILCs created a cytokine microenvironment in the meninges which favored the loss of IL-17A-single producing 2D2 CD4$^+$ T cells and promoted the differentiation of IFN-γ-single producing 2D2 CD4$^+$ T cells. Interestingly, we detected a higher frequency of GM-CSF-producing 2D2 CD4$^+$ T cells in the meninges and parenchyma of *Tbx21*$^{f/f}$ and *Tbx21*$^{f/f}$ NKp46-Cre$^+$ mice (Supplementary Fig. 8). Although T cell-derived GM-CSF is required for EAE[44, 45], it is not sufficient to drive neuroinflammation in *Tbx21*$^{f/f}$ NKp46-Cre$^+$ mice. Importantly, the extent of myelin destruction and the frequency of apoptotic (TUNEL$^+$) cells was significantly decreased in the spinal cords of *Tbx21*$^{f/f}$ NKp46-Cre$^+$ mice compared with *Tbx21*$^{f/f}$ controls (Fig. 8d,e), indicating that NKp46-lineage specific deletion of T-bet significantly reduced the extent of immune-mediated damage driven by autoreactive CD4$^+$ T_H17 cells. Collectively, these results demonstrate that T-bet-dependent NKp46$^+$ ILCs are required for optimal reactivation, parenchymal invasion and maintenance of myelin-reactive CD4$^+$ T_H17 cells in the CNS tissue.

DISCUSSION

By employing a reductionist and *in vivo* approach, we demonstrate a previously unappreciated requirement for T-bet-dependent NKp46$^+$ ILCs in the pathogenesis of T_H17-driven neuroinflammation. EAE is a neuroinflammatory disease initiated by tissue-invading leukocytes[34]. We found that myelin-reactive, pathogenic CD4$^+$ T_H17 cells invaded and triggered extensive lesions throughout the CNS tissue in immunocompetent hosts while they were absent from the CNS parenchyma of T-bet-deficient hosts. Similarly, adoptive transfer of 2D2 wild-type T_H17 into mice depleted of NK1.1$^+$ cells or into mice with NKp46-lineage specific deletion of T-bet resulted in significantly reduced disease incidence underscoring the importance of NK1.1$^+$ NKp46$^+$ ILCs in the pathology of T_H17-mediated neuroinflammation. This group of innate lymphocytes includes NK cells, ILC1 and the NKp46$^+$ subset of ILC3s[23, 24]. All three subsets of NKp46$^+$ ILCs were readily detected in the meninges of wild-type mice during EAE, suggesting that these innate immune cells could have a local effect on tissue-specific immune responses in the CNS.

T-bet expression impacts many aspects of NK cell homeostasis and function[22, 27, 46, 47]. This raised a possibility that *Tbx21*$^{-/-}$ and *Tbx21*$^{f/f}$ NKp46-Cre^{+} mice may be protected from T_H17-mediated disease due to peripheral deficiency of NK cells. However, NK cell-deficient mice developed as severe paralysis as NK cell-sufficient mice, indicating that NK cells do not have a major effect on the immunopathogenesis of EAE and that the pathogenic function of T-bet maps to ILC1 and/or the NKp46^{+} subset of ILC3s. Our results do not exclude the possibility that NKp46^{+} ILC subsets may function redundantly. Dissecting the contributions of each NKp46^{+} ILC subset in regulating CNS-specific immune responses by generating mice with single or multiple ILC deficiencies will be an important area of future investigations.

Our findings have also raised the question of how T-bet-dependent NKp46^{+} ILCs control the onset of T_H17 cell-mediated neuroinflammation. Pathology of EAE is triggered by the immune cell invasion of the CNS parenchyma, which is a highly regulated process. We think that T-bet-dependent NKp46^{+} ILCs create a microenvironment in the meninges that facilitates T cell migration across the parenchymal border, primarily through the induction of pro-inflammatory cytokines (IL-1β, IL-6, TNF-α, LT-α and IL-23), which then stimulate the expression of MMPs and chemokines. A recent study has shown that the abundance of chemokines and the expression and activity of MMPs were enhanced by encephalitogenic CD4^{+} T_H17 cells, which produced high levels of IL-17A/TNFα and low levels of IFN-γ[40]. We observed that the microenvironment in the meninges of *Tbx21*$^{f/f}$ NKp46-Cre^{+} skewed the cytokine production by 2D2 CD4^{+} T cells from IL-17A to IFN-γ, indicating that the expression of chemokines and MMPs might be adversely affected by this shift in cytokine production. Consistent with that hypothesis, we found a significant reduction in the levels of chemokines and MMPs in the meninges of *Tbx21*$^{f/f}$ NKp46-Cre^{+} mice. Our findings also accentuate the developmental instability of CD4^{+} T_H17 cells, which require constant exposure to T_H17-inducing cytokines to maintain their T_H17-ness.

In summary, we propose that the primary function of T-bet-dependent NKp46^{+} ILCs is to promote parenchymal infiltration of myelin-reactive CD4^{+} T cells and to maintain the functional stability of the T_H17 cells by coordinating appropriate inflammatory responses in the meninges. Additionally, we demonstrate that NKp46-lineage specific deletion of T-bet was sufficient to significantly reduce the extent of immune-mediated damage driven by autoreactive CD4^{+} T_H17 cells. New treatments for neuroinflammation should be designed to selectively limit responses of T-bet-dependent NKp46^{+} ILCs in the CNS.

ONLINE METHODS

Mice

C57BL/6 (WT), *Tbx21*$^{-/-}$, *Eomes*$^{f/f}$, 2D2 TCR-transgenic, Vav1-Cre^{+}, CD4-Cre^{+}, CD11c-Cre^{+} and R26R-YFP mice were purchased from the Jackson Laboratory. Mutant strains were previously described: NKp46-Cre^{+}[48], Tbet-ZsGreen reporter[17], *Tbx21*$^{f/f}$[49] and Actin-OFP[50]. Male and female mice were used between 7–12 weeks of age. Animal experiments were approved by the NCI Institute Animal Care and Use Committee. All mice were maintained in accordance with US National Institutes of Health guidelines.

In vitro differentiation of 2D2 T_H17 cells for adoptive transfer

Naïve 2D2 TCR-transgenic $CD4^+$ T cells from spleen and lymph nodes of 2D2 wild-type or 2D2 *Tbx21*$^{-/-}$ mice were electronically sorted ($CD4^+V_\beta11^+CD62L^{hi}$), and activated under T_H17 polarizing conditions with the following: anti-CD3 (2.5 μg/ml) (145-2C11, BioXCell), anti-IL-4 (20 μg/ml) (11B11, BioXCell), anti-IFN-γ (20 μg/ml) (XMG1.2, BioXCell), mIL-6 (30 ng/ml) (Miltenyi Biotec), hTGF-β1 (3 ng/ml) (Miltenyi Biotec) in the presence of irradiated wild-type splenocytes at 5:1 ratio. After 60 h of activation, mIL-23 (10 ng/ml; R&D Systems) was added. On day 5 of culture, cells were reactivated on plates pre-coated with 2 μg/ml of anti-CD3 and anti-CD28 (PV1, BioXCell), for an additional 48 h, prior to adoptive transfer.

Active and passive induction of EAE and disease analysis

Active EAE was induced by immunization with the myelin oligodendrocyte glycoprotein (MOG) peptide amino acids 35–55 (MEVGWYRSPFSRVVHLYRNGK). 100 μg MOG_{35-55} peptide was emulsified in complete Freund's adjuvant supplemented with *M. tuberculosis* extract H37Ra (Difco), and injected subcutaneously. Mice received 150 ng pertussis toxin (List Biological Laboratories) intraperitoneally on days 0 and 2. Passive transfer EAE was induced by injecting 2D2 T_H17-polarized cells (as described above) intravenously into recipient mice at 5–7.5 × 10^6 cells/mouse. For NK depletion experiments, 0.5 mg/dose of purified anti-NK1.1 (clone PK136, BioXCell) was injected intravenously into mice on days −5/−3/−1 prior to 2D2 adoptive transfer, and additionally every 3 days from day 1 post-2D2 transfer. Classical EAE symptoms were scored daily according to standard criteria: 0, asymptomatic; 1, flaccid tail; 2, hind limb weakness and impaired righting ability; 3, hind limb paralysis; 4, front and hind limb paralysis; 5, moribund or death.

Isolation of CNS parenchymal and meningeal cells

For isolation of CNS-infiltrating cells for flow cytometry, brain and spinal cord tissues were minced and digested using 2.5 mg/ml collagenase D (Roche) and 1 mg/ml DNase I (Roche) for 30 min at 37 °C. Tissues were mechanically disrupted using a gentleMACS Dissociator (Miltenyi), filtered through 70 μm mesh strainers, and centrifuged through a Percoll density gradient (38% and 70%). Mononuclear cells in the interphase were removed, washed and resuspended in culture medium for analysis by flow cytometry. For isolation of spinal cord meningeal cells, mice were transcardially perfused with PBS and the meninges was extracted from the spinal column after removal of the spinal cord parenchyma. Meninges tissues were digested using 2.5 mg/ml collagenase D and 0.1 mg/ml DNase I for 30 min at 37 °C, then filtered through 70 μm mesh strainers to generate single-cell suspensions.

Antibodies

The following antibody clones were used for flow cytometry: B220 (RA3-6B2); CCR6 (29-2L17); CD11b (M1/70); CD11c (HL3); CD16/32 Fc Block (2.4G2); CD206 (C068C2); CD3ε (145-2C11); CD4 (RM4-5); CD45 (30-F11); CD45.2 (104); CD49b (DX5); CD54/ICAM-1 (YN1/1.7.4); CD80 (16-10A1); CXCR4 (2B11); F4/80 (BM8); IFN-γ (XMG1.2); IL-17A (TC11-18H10.1); $Itg\alpha_4$/CD49d (R1-2); $Itg\alpha_L$/CD11a (M17/4); Ki67 (B56); Ly-6C (HK1.4); Ly-6G (1A8); I-A/I-E (M5); NK1.1 (PK136); NKp46 (29A1.4); Thy1.2 (30-H12);

TCRβ (H57); $V_β$11 TCR (RR3-15); RORγt (AFKJS-9); CD127/IL-7Rα (A7R34); Gr1 (RB6-8C5); TCRγδ (GL3). The following antibody clones were used for immunohistology: CD4 (RM4-5); myelin basic protein (SMI-94).

Flow cytometry

For intracellular cytokine staining of cell suspensions from the spleen, lung, or CNS, cells were first stimulated *ex vivo* for a total of 4 h with PMA (50 ng/ml; Sigma) and ionomycin (1 μM; Sigma), including the addition of monensin (3 μM) to block secretion in the last 2 h of stimulation. Cells were stained with fixable live/dead dye according to the manufacturer's protocol (Life Technologies), then stained with antibodies against surface markers in the presence of anti-CD16/32 Fc Block (2.4G2) for 30 min at 4 °C. After surface marker staining, cells were fixed and permeabilized in Cytofix/Cytoperm solution (BD Biosciences) for 30 min prior to intracellular staining of cytokines for 30 min at 4 °C. Ki67 intranuclear staining was performed following fixation and permeabilization using the Foxp3/ Transcription Factor Staining kit from eBioscience. Samples were acquired on a BD LSRFortessa or LSRII flow cytometer (BD Biosciences), and FlowJo software (TreeStar) was used for data analysis.

Immunohistology and TUNEL quantification

Mice were transcardially perfused with 2% or 4% paraformaldehyde (PFA) for *in vivo* fixation. Spinal cords were extracted and placed in 2% PFA at 4°C for 12 h of additional fixation, then transferred to 30% sucrose for >24h before embedding in Tissue-Tek OCT compound (Sakura) for cryopreservation. Frozen tissues were cryosectioned into 12 μm slices for immunostaining. Prior to staining, sections were re-fixed with 1% PFA for 10 min, washed with PBS, and blocked by incubating with 1% bovine serum albumin and 5% normal goat serum for 2 h at 23 °C. Primary antibodies against CD4 and myelin basic protein (MBP) were incubated for at least 12 h at 4 °C. Fluorescently labeled secondary goat antibodies (Jackson Immuno) against the relevant species were incubated for 2 h at 23 °C. After washing and counterstaining with DAPI (Life Technologies), slides were mounted with Vectashield Antifade Mounting Medium (Vector Laboratories) and sealed. For negative staining controls, sections were incubated with secondary antibodies after omitting primary antibodies. For the detection of apoptotic cells by TUNEL assay, the ApopTag Fluorescein *In Situ* Apoptosis Detection Kit (Millipore) was used according to the manufacturer's protocol. Images were acquired using a Zeiss LSM880 confocal microscope and processed using Zen imaging software (Zeiss). Multiple slices from each experimental mouse were examined to ensure the reproducibility of histological staining. The quantification of $TUNEL^+$ cells from histological images was performed using Zen imaging software in a blinded manner by the EIB Microscopy Facility (NCI), normalized to the total tissue section area, and expressed as # cells/mm^2.

Histo-cytometry

z-stack images of whole mount spinal cord meninges were collected using Olympus FV1200 laser scanning confocal microscope using the 405, 488, 559, and 635 nm laser lines, and objectives with 4× magnification (0.16 NA), and 20× magnification (0.75 NA), 10 μm-step size at a voxel density of 1024×1024. Fluorophore emission was collected on 4 side window

PMT with sequential laser excitation to minimize spectral spillover. The extended field of view images were acquired using the multi-area timelapse module of the image acquisition software (Olympus fluoview Ver.4.2a). The grid of images was stitched using the same module to a single large image. DAPI, YFP, OFP and Alexa-647 channels were collected to detect nucleated cells, NKp46^{+} cells, 2D2 CD4^{+} T cells and I-A/I-E^{+} APCs, respectively. For YFP, OFP and Alexa-647 channels, threshold identification, voxel gating and spot creation without background subtraction were performed using the Spot Creation Wizard (Imaris software) that provided automatic threshold identification of the positively stained cells based on the 'Quality' parameter. The estimated diameter used for thresholding was set as 15 μm. For the spots corresponding to each cell type, all 4 channel statistics (DAPI, YFP, OFP, Alexa-647) were exported into Excel (Microsoft) and converted to a csv file for direct visualization in FlowJo v10 (Treestar). For each cell type, DAPI-positive spots were then selected against debris based on value-based visual thresholding and were discriminated on a biexponential-scale. Those actual cells were then plotted in color on a 10^{-2}–10^{4} biexponential-scale in the dot-plots shown in Fig. 5. Irrelevant populations (NKp46^{+} spots for I-A/I-E^{+} APCs and 2D2 CD4^{+} T dot-plots, and I-A/I-E^{+} spots for NKp46^{+} dot-plot) before DAPI-positive selection are plotted in grey to show negative populations.

Quantitative RT-PCR on tissue homogenates

Mice were transcardially perfused with PBS, and the spinal cord parenchyma and spinal cord meningeal tissue were harvested. Tissues were immediately immersed in QIAzol Lysis Reagent (Qiagen) with zirconia/silica beads (Biospec), mechanically homogenized, and stored at −80 °C. RNA isolation was performed by phenol-chloroform extraction, and reverse transcription was performed using MultiScribe Reverse Transcriptase (Thermo Fisher). RT-PCR was carried out using the SYBR Green PCR system (Thermo Fisher), and analyzed on a QuantStudio 6 Flex instrument (Thermo Fisher). mRNA expression was calculated by the ΔCt method, relative to housekeeping genes *Hprt* or *Rpl13*. RT-PCR primer sequences are listed in the Supplementary Table 1.

Statistics

Statistical significance was calculated by unpaired two-tailed Student's *t*-test or 2-way ANOVA, as noted in figure legends, using GraphPad Prism software. All data are presented as mean ± standard error of mean (s.e.m.), unless otherwise noted.

Supplementary Material

Refer to Web version on PubMed Central for supplementary material.

Acknowledgments

We thank Y. Belkaid and A. Singer for critical review of the manuscript, S. Sharrow, L. Granger and A. Adams for flow cytometry and cell sorting, T. Loo for technical assistance and the members of the A. Singer and H. Park laboratories for discussions. S. Reiner (Columbia University) generously provided *Tbx21*$^{f/f}$ mice. This study was supported by the Intramural Research Program of the US National Institutes of Health, National Cancer Institute, Center for Cancer Research (ZIA BC 011431 and ZIA BC 011432) and National Institute of Neurological Disorders and Stroke.

References

1. McFarland HF, Martin R. Multiple sclerosis: a complicated picture of autoimmunity. Nat Immunol. 2007; 8:913–919. [PubMed: 17712344]
2. Park H, et al. A distinct lineage of CD4 T cells regulates tissue inflammation by producing interleukin 17. Nat Immunol. 2005; 6:1133–1141. [PubMed: 16200068]
3. Langrish CL, et al. IL-23 drives a pathogenic T cell population that induces autoimmune inflammation. J Exp Med. 2005; 201:233–240. [PubMed: 15657292]
4. McGeachy MJ, et al. The interleukin 23 receptor is essential for the terminal differentiation of interleukin 17-producing effector T helper cells in vivo. Nat Immunol. 2009; 10:314–324. [PubMed: 19182808]
5. Cua DJ, et al. Interleukin-23 rather than interleukin-12 is the critical cytokine for autoimmune inflammation of the brain. Nature. 2003; 421:744–748. [PubMed: 12610626]
6. Schlager C, et al. Effector T-cell trafficking between the leptomeninges and the cerebrospinal fluid. Nature. 2016; 530:349–353. [PubMed: 26863192]
7. Bettelli E, et al. Loss of T-bet, but not STAT1, prevents the development of experimental autoimmune encephalomyelitis. J Exp Med. 2004; 200:79–87. [PubMed: 15238607]
8. Lovett-Racke AE, et al. Silencing T-bet defines a critical role in the differentiation of autoreactive T lymphocytes. Immunity. 2004; 21:719–731. [PubMed: 15539157]
9. Lazarevic V, Glimcher LH, Lord GM. T-bet: a bridge between innate and adaptive immunity. Nat Rev Immunol. 2013; 13:777–789. [PubMed: 24113868]
10. Lazarevic V, Glimcher LH. T-bet in disease. Nat Immunol. 2011; 12:597–606. [PubMed: 21685955]
11. Lee Y, et al. Induction and molecular signature of pathogenic TH17 cells. Nat Immunol. 2012; 13:991–999. [PubMed: 22961052]
12. Wang Y, et al. The transcription factors T-bet and Runx are required for the ontogeny of pathogenic interferon-gamma-producing T helper 17 cells. Immunity. 2014; 40:355–366. [PubMed: 24530058]
13. Yang Y, et al. T-bet is essential for encephalitogenicity of both Th1 and Th17 cells. J Exp Med. 2009; 206:1549–1564. [PubMed: 19546248]
14. Ghoreschi K, et al. Generation of pathogenic T(H)17 cells in the absence of TGF-beta signalling. Nature. 2010; 467:967–971. [PubMed: 20962846]
15. Odoardi F, et al. T cells become licensed in the lung to enter the central nervous system. Nature. 2012; 488:675–679. [PubMed: 22914092]
16. Flugel A, et al. Migratory activity and functional changes of green fluorescent effector cells before and during experimental autoimmune encephalomyelitis. Immunity. 2001; 14:547–560. [PubMed: 11371357]
17. Zhu J, et al. The transcription factor T-bet is induced by multiple pathways and prevents an endogenous Th2 cell program during Th1 cell responses. Immunity. 2012; 37:660–673. [PubMed: 23041064]
18. Greter M, et al. Dendritic cells permit immune invasion of the CNS in an animal model of multiple sclerosis. Nat Med. 2005; 11:328–334. [PubMed: 15735653]
19. Kivisakk P, et al. Localizing central nervous system immune surveillance: meningeal antigen-presenting cells activate T cells during experimental autoimmune encephalomyelitis. Ann Neurol. 2009; 65:457–469. [PubMed: 18496841]
20. McMahon EJ, Bailey SL, Castenada CV, Waldner H, Miller SD. Epitope spreading initiates in the CNS in two mouse models of multiple sclerosis. Nat Med. 2005; 11:335–339. [PubMed: 15735651]
21. Fuchs A, et al. Intraepithelial type 1 innate lymphoid cells are a unique subset of IL-12- and IL-15-responsive IFN-gamma-producing cells. Immunity. 2013; 38:769–781. [PubMed: 23453631]
22. Gordon SM, et al. The transcription factors T-bet and Eomes control key checkpoints of natural killer cell maturation. Immunity. 2012; 36:55–67. [PubMed: 22261438]

23. Klose CS, et al. Differentiation of type 1 ILCs from a common progenitor to all helper-like innate lymphoid cell lineages. Cell. 2014; 157:340–356. [PubMed: 24725403]
24. Klose CS, et al. A T-bet gradient controls the fate and function of CCR6-RORgammat+ innate lymphoid cells. Nature. 2013; 494:261–265. [PubMed: 23334414]
25. Rankin LC, et al. The transcription factor T-bet is essential for the development of NKp46+ innate lymphocytes via the Notch pathway. Nat Immunol. 2013; 14:389–395. [PubMed: 23455676]
26. Sciume G, et al. Distinct requirements for T-bet in gut innate lymphoid cells. J Exp Med. 2012; 209:2331–2338. [PubMed: 23209316]
27. Townsend MJ, et al. T-bet regulates the terminal maturation and homeostasis of NK and Valpha14i NKT cells. Immunity. 2004; 20:477–494. [PubMed: 15084276]
28. Morandi B, et al. Role of natural killer cells in the pathogenesis and progression of multiple sclerosis. Pharmacol Res. 2008; 57:1–5. [PubMed: 18182304]
29. Winkler-Pickett R, et al. In vivo regulation of experimental autoimmune encephalomyelitis by NK cells: alteration of primary adaptive responses. J Immunol. 2008; 180:4495–4506. [PubMed: 18354171]
30. Liu Q, et al. Neural stem cells sustain natural killer cells that dictate recovery from brain inflammation. Nat Neurosci. 2016; 19:243–252. [PubMed: 26752157]
31. Bielekova B, et al. Regulatory CD56(bright) natural killer cells mediate immunomodulatory effects of IL-2Ralpha-targeted therapy (daclizumab) in multiple sclerosis. Proc Natl Acad Sci U S A. 2006; 103:5941–5946. [PubMed: 16585503]
32. Hao J, et al. Central nervous system (CNS)-resident natural killer cells suppress Th17 responses and CNS autoimmune pathology. J Exp Med. 2010; 207:1907–1921. [PubMed: 20696699]
33. Pikovskaya O, et al. Cutting Edge: Eomesodermin Is Sufficient To Direct Type 1 Innate Lymphocyte Development into the Conventional NK Lineage. J Immunol. 2016; 196:1449–1454. [PubMed: 26792802]
34. Becher B, Spath S, Goverman J. Cytokine networks in neuroinflammation. Nat Rev Immunol. 2017; 17:49–59. [PubMed: 27916979]
35. Rothhammer V, et al. Th17 lymphocytes traffic to the central nervous system independently of alpha4 integrin expression during EAE. J Exp Med. 2011; 208:2465–2476. [PubMed: 22025301]
36. Reboldi A, et al. C-C chemokine receptor 6-regulated entry of TH-17 cells into the CNS through the choroid plexus is required for the initiation of EAE. Nat Immunol. 2009; 10:514–523. [PubMed: 19305396]
37. Bauer M, et al. Beta1 integrins differentially control extravasation of inflammatory cell subsets into the CNS during autoimmunity. Proc Natl Acad Sci U S A. 2009; 106:1920–1925. [PubMed: 19179279]
38. Dungan LS, McGuinness NC, Boon L, Lynch MA, Mills KH. Innate IFN-gamma promotes development of experimental autoimmune encephalomyelitis: a role for NK cells and M1 macrophages. Eur J Immunol. 2014; 44:2903–2917. [PubMed: 25056715]
39. Kipnis J. Multifaceted interactions between adaptive immunity and the central nervous system. Science. 2016; 353:766–771. [PubMed: 27540163]
40. Song J, et al. Focal MMP-2 and MMP-9 activity at the blood-brain barrier promotes chemokine-induced leukocyte migration. Cell Rep. 2015; 10:1040–1054. [PubMed: 25704809]
41. Chiang EY, et al. Targeted depletion of lymphotoxin-alpha-expressing TH1 and TH17 cells inhibits autoimmune disease. Nat Med. 2009; 15:766–773. [PubMed: 19561618]
42. Chung Y, et al. Critical regulation of early Th17 cell differentiation by interleukin-1 signaling. Immunity. 2009; 30:576–587. [PubMed: 19362022]
43. Pikor NB, et al. Integration of Th17- and Lymphotoxin-Derived Signals Initiates Meningeal-Resident Stromal Cell Remodeling to Propagate Neuroinflammation. Immunity. 2015; 43:1160–1173. [PubMed: 26682987]
44. Codarri L, et al. RORgammat drives production of the cytokine GM-CSF in helper T cells, which is essential for the effector phase of autoimmune neuroinflammation. Nat Immunol. 2011; 12:560–567. [PubMed: 21516112]

45. El-Behi M, et al. The encephalitogenicity of T(H)17 cells is dependent on IL-1- and IL-23-induced production of the cytokine GM-CSF. Nat Immunol. 2011; 12:568–575. [PubMed: 21516111]
46. Jenne CN, et al. T-bet-dependent S1P5 expression in NK cells promotes egress from lymph nodes and bone marrow. J Exp Med. 2009; 206:2469–2481. [PubMed: 19808259]
47. van Helden MJ, et al. Terminal NK cell maturation is controlled by concerted actions of T-bet and Zeb2 and is essential for melanoma rejection. J Exp Med. 2015; 212:2015–2025. [PubMed: 26503444]
48. Narni-Mancinelli E, et al. Fate mapping analysis of lymphoid cells expressing the NKp46 cell surface receptor. Proc Natl Acad Sci U S A. 2011; 108:18324–18329. [PubMed: 22021440]
49. Intlekofer AM, et al. Anomalous type 17 response to viral infection by CD8+ T cells lacking T-bet and eomesodermin. Science. 2008; 321:408–411. [PubMed: 18635804]
50. Gossa S, Nayak D, Zinselmeyer BH, McGavern DB. Development of an immunologically tolerated combination of fluorescent proteins for in vivo two-photon imaging. Sci Rep. 2014; 4:6664. [PubMed: 25322934]

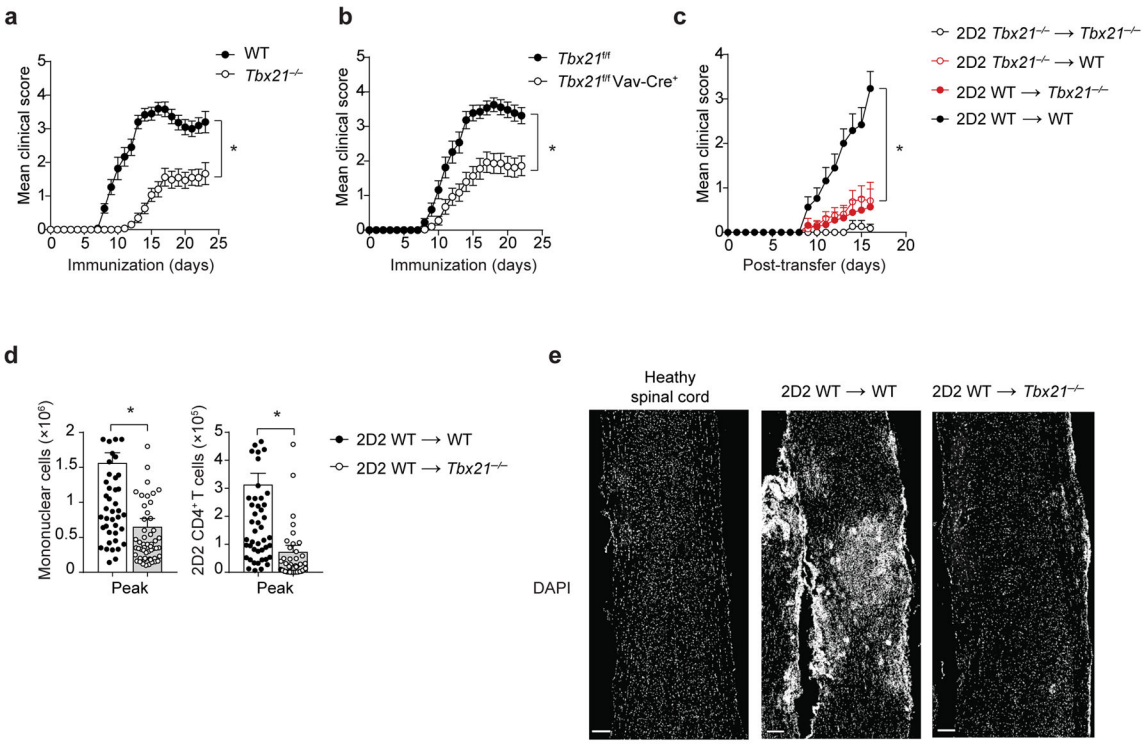

Figure 1.

T-bet expression in T cells is insufficient to cause EAE. (**a–b**) Mean clinical scores in wild-type (WT) versus *Tbx21*$^{-/-}$ mice (**a**), or *Tbx21*$^{f/f}$ versus *Tbx21*$^{f/f}$ Vav-Cre^{+} mice (**b**), immunized with MOG_{35-55}/CFA and pertussis toxin. (**c**) Mean clinical scores in *Tbx21*$^{-/-}$ or WT mice receiving 5×10^6 2D2 *Tbx21*$^{-/-}$ or 2D2 WT T_H17 cells. (**d**) Enumeration of total CNS-infiltrating mononuclear cells or CNS-infiltrating 2D2 CD4^{+} T cells (CD4^{+}V$_{\beta}$11^{+}) at the peak of EAE disease (day 15–17 post-transfer), in *Tbx21*$^{-/-}$ or WT recipients of 2D2 WT T_H17 cells ($5–7.5 \times 10^6$), analyzed by flow cytometry. (**e**) DAPI staining of spinal cord longitudinal sections from a naïve healthy mouse or *Tbx21*$^{-/-}$ or WT recipients of 2D2 WT T_H17 cells (7.5×10^6). Scale bar, 200 μm. *, $P < 0.0001$ (two-way ANOVA (**a–c**) or two-tailed Student's *t*-test (**d**)). Data are combined from three independent experiments (**a**; mean ± s.e.m. of $n = 30$ mice per group), four independent experiments (**b**; mean ± s.e.m. of $n = 28$ mice per group), five independent experiments (**c**; mean ± s.e.m. of $n = 15 – 20$ mice per group) and 12 independent experiments (**d**; mean ± s.e.m. of $n = 54$, 57 mice per group). Histological images are representative of three independent experiments ($n = 6$, 9 mice per group).

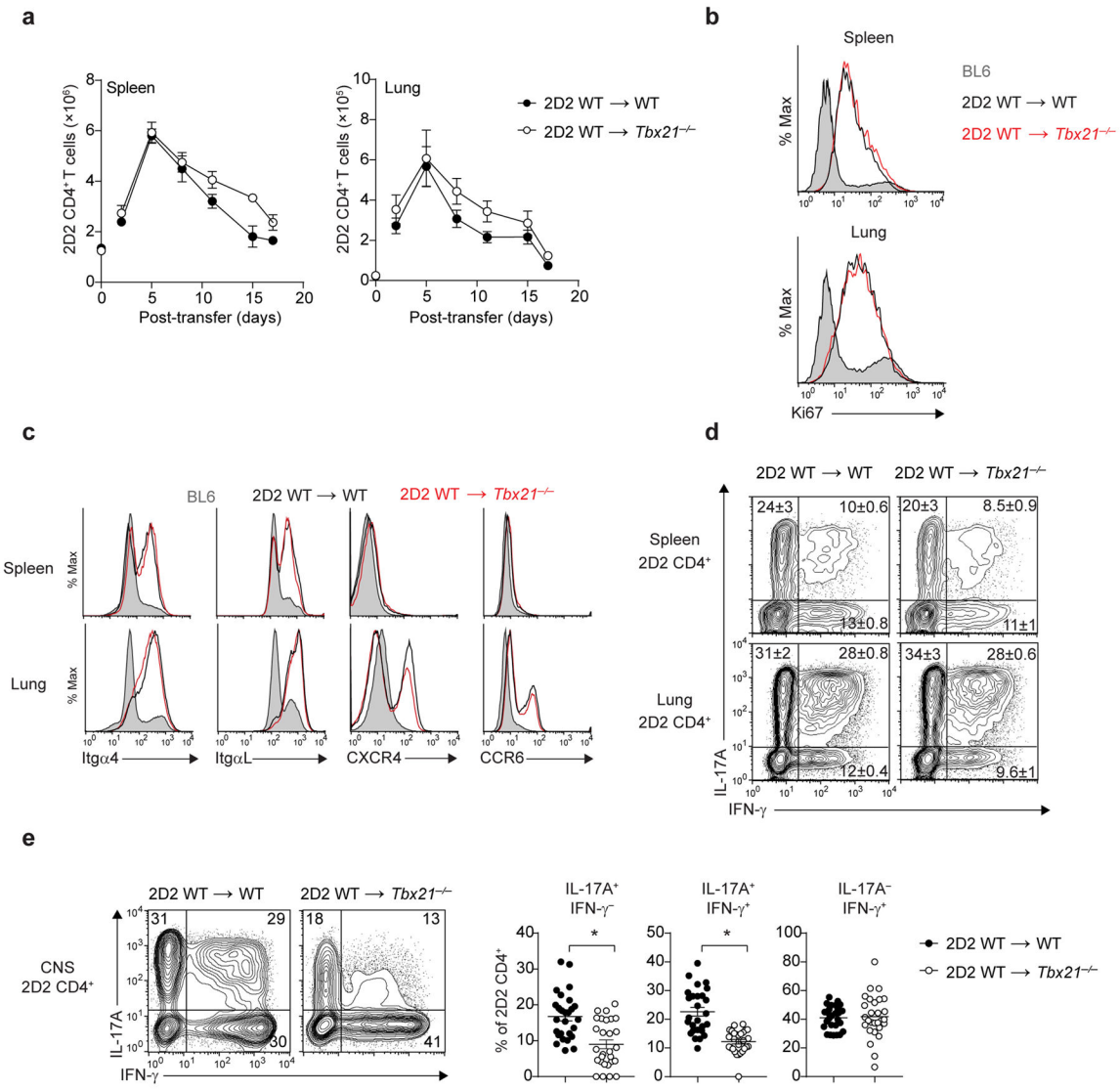

Figure 2.

Peripheral licensing of CD4$^+$ T_H17 cells in *Tbx21*$^{-/-}$ host. (**a**) Time-course analysis quantifying the number of 2D2 CD4$^+$ T cells (CD4$^+$V$_\beta$11$^+$) in the spleens or lungs of *Tbx21*$^{-/-}$ or WT mice, following adoptive transfer of 7.5 × 10^6 2D2 WT T_H17 cells. (**b**) Ki67 intracellular staining of 2D2 CD4$^+$ T cells (CD3$^+$CD4$^+$V$_\beta$11$^+$) trafficking through the spleens or lungs of *Tbx21*$^{-/-}$ or WT mice five days post-adoptive transfer (n = 5 mice per group). Histograms are overlaid with Ki67 expression in endogenous WT (BL6) CD4$^+$ T cells (shaded). (**c**) Expression of migratory receptors on 2D2 CD4$^+$ T cells trafficking through the spleens or lungs of *Tbx21*$^{-/-}$ or WT mice five days post-adoptive transfer. Histograms are overlaid with expression detected on endogenous WT (BL6) CD4$^+$ T cells (shaded). (**d**) Intracellular cytokine staining of 2D2 CD4$^+$ T cells from the spleens or lungs of *Tbx21*$^{-/-}$ or WT mice, five days post-adoptive transfer. (**e**) Intracellular cytokine staining of 2D2 CD4$^+$ T cells from the CNS of *Tbx21*$^{-/-}$ or WT mice at the peak of EAE disease (day 15–17 post-transfer). *, $P < 0.0001$ (two-tailed Student's t-test). Data are representative

of two independent experiments (**a**,**d**; mean ± s.e.m. of $n = 6$ mice per group), three independent experiments (**c**; $n = 10$ mice per group) or five independent experiments (**e**; mean ± s.e.m. of $n = 27$ mice per group).

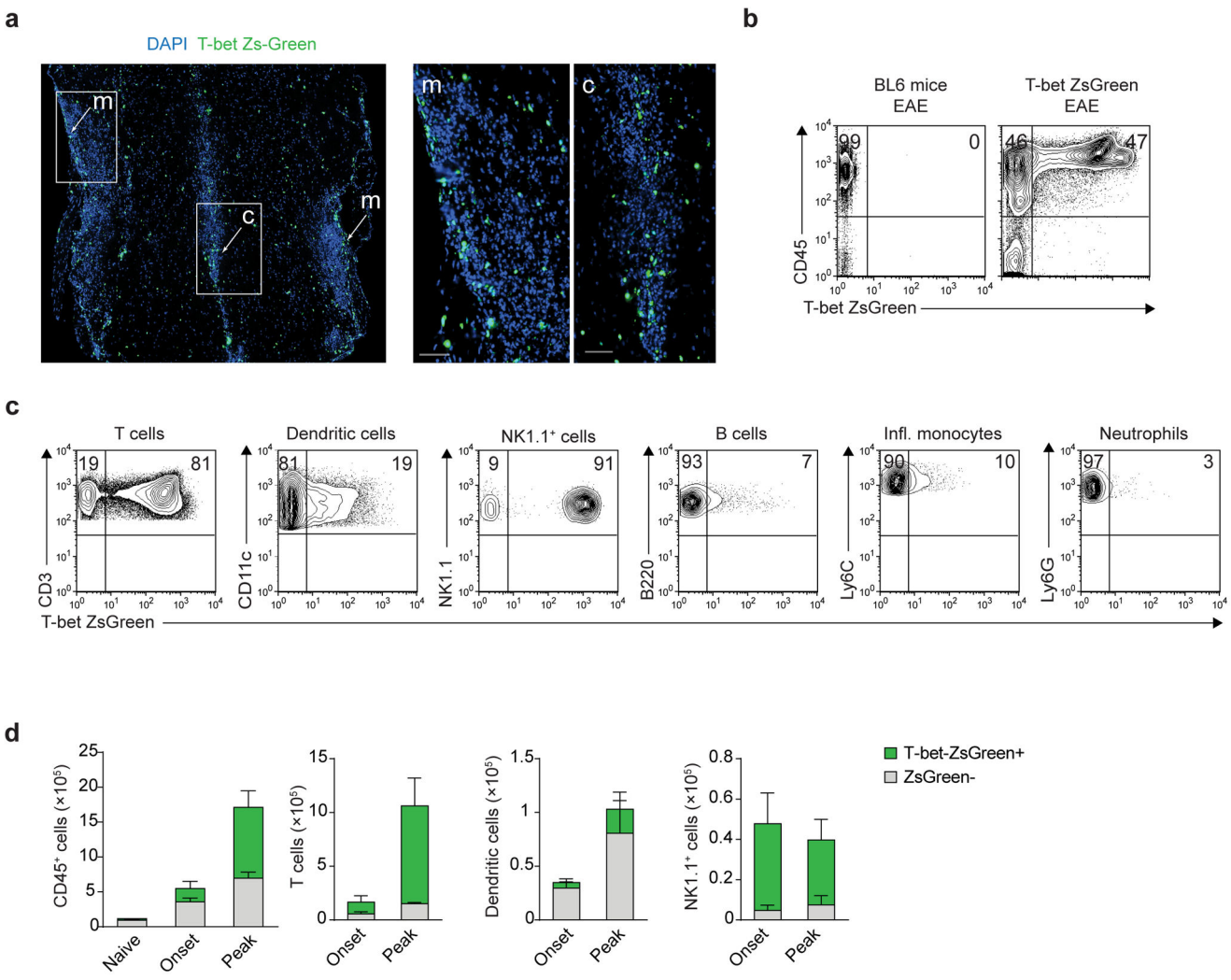

Figure 3.

T-bet-expressing cells in the CNS during EAE. (**a**) DAPI staining of spinal cord longitudinal sections from T-bet-ZsGreen reporter mice immunized with MOG_{35-55}/CFA and pertussis toxin, harvested at the peak of EAE disease (day 14 post-immunization). Inset images show ZsGreen reporter$^+$ cells in the meninges (m) and central canal (c) of the spinal cord. Scale bar, 50 μm. (**b**) Flow cytometric analysis of the CNS of WT (BL6) or T-bet ZsGreen reporter mice immunized with MOG_{35-55}/CFA and pertussis toxin. Analysis is gated on total live cells. (**c**) Analysis of T-bet ZsGreen expression in CNS-infiltrating immune cell populations from T-bet ZsGreen reporter mice immunized with MOG_{35-55}/CFA and pertussis toxin. Immune cell subsets were gated on live CD45$^+$ cells, then further identified as follows: T cells, MHCII$^-$CD3$^+$; dendritic cells, CD3$^-$MHCII$^+$CD11c$^+$; NK1.1$^+$ innate cells, CD3$^-$MHCII$^-$NK1.1$^+$; B cells, CD3$^-$MHCII$^+$B220$^+$; inflammatory monocytes, CD3$^-$CD11b$^+$Ly6C^{hi}Ly6G$^-$; neutrophils, CD3$^-$CD11b$^+$Ly6C^{int}Ly6G$^+$. (**d**) Quantitation by flow cytometry of T-bet-expressing CD45$^+$ immune cells, T cells, dendritic cells or NK1.1$^+$ innate cells from the CNS of T-bet ZsGreen reporter mice immunized with MOG_{35-55}/CFA and pertussis toxin. CNS-infiltrating cells were harvested at the onset (day 7) or peak of

EAE disease (day 13–14 post-immunization) and stained for lineage-specific markers as in (**c**). Data in (**b–d**) are combined from 2–3 independent experiments, using 5 pooled mice per group per experiment; data are presented as mean ± s.e.m (**d**). Histological images are representative of 2 independent experiments (n = 4 mice).

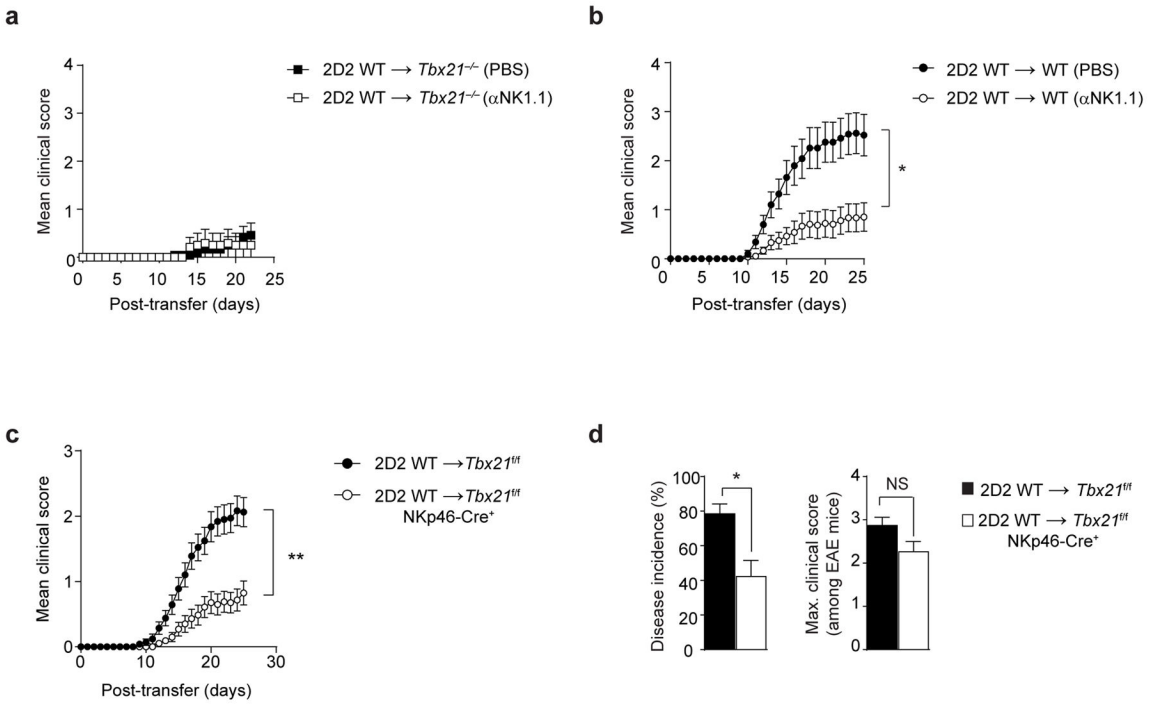

Figure 4.

T-bet-dependent NKp46^{+} ILCs initiate T_H17-mediated EAE. (**a–b**) Mean clinical scores of *Tbx21*$^{-/-}$ and WT mice following the adoptive transfer of 7.5×10^6 2D2 WT T_H17 cells, with anti-NK1.1-mediated depletion (αNK1.1) or PBS control injections performed before and during EAE disease. Detailed description of the anti-NK1.1 (clone PK136) depletion regimen is described in Supplementary Fig. 3. (**c**) Mean clinical scores of *Tbx21*$^{f/f}$ or *Tbx21*$^{f/f}$ NKp46-Cre^{+} mice following adoptive transfer of 7.5×10^6 2D2 WT T_H17 cells. (**d**) The disease incidence in each independent experiment (percentage of mice demonstrating EAE symptoms) and the maximum clinical score among EAE symptomatic mice only. NS, *P > 0.05; *, P < 0.01*; ** *P < 0.0001* (two-way ANOVA (**b**,**c**) or two-tailed Student's *t*-test (**d**)). Data are representative of 2 independent experiments (**a**; mean ± s.e.m. of $n = 12$ mice per group), four independent experiments (**b**; mean ± s.e.m. of $n = 25$, 27 mice per group) and 8 independent experiments (**c**,**d**; mean ± s.e.m. of $n = 37$, 49 mice per group).

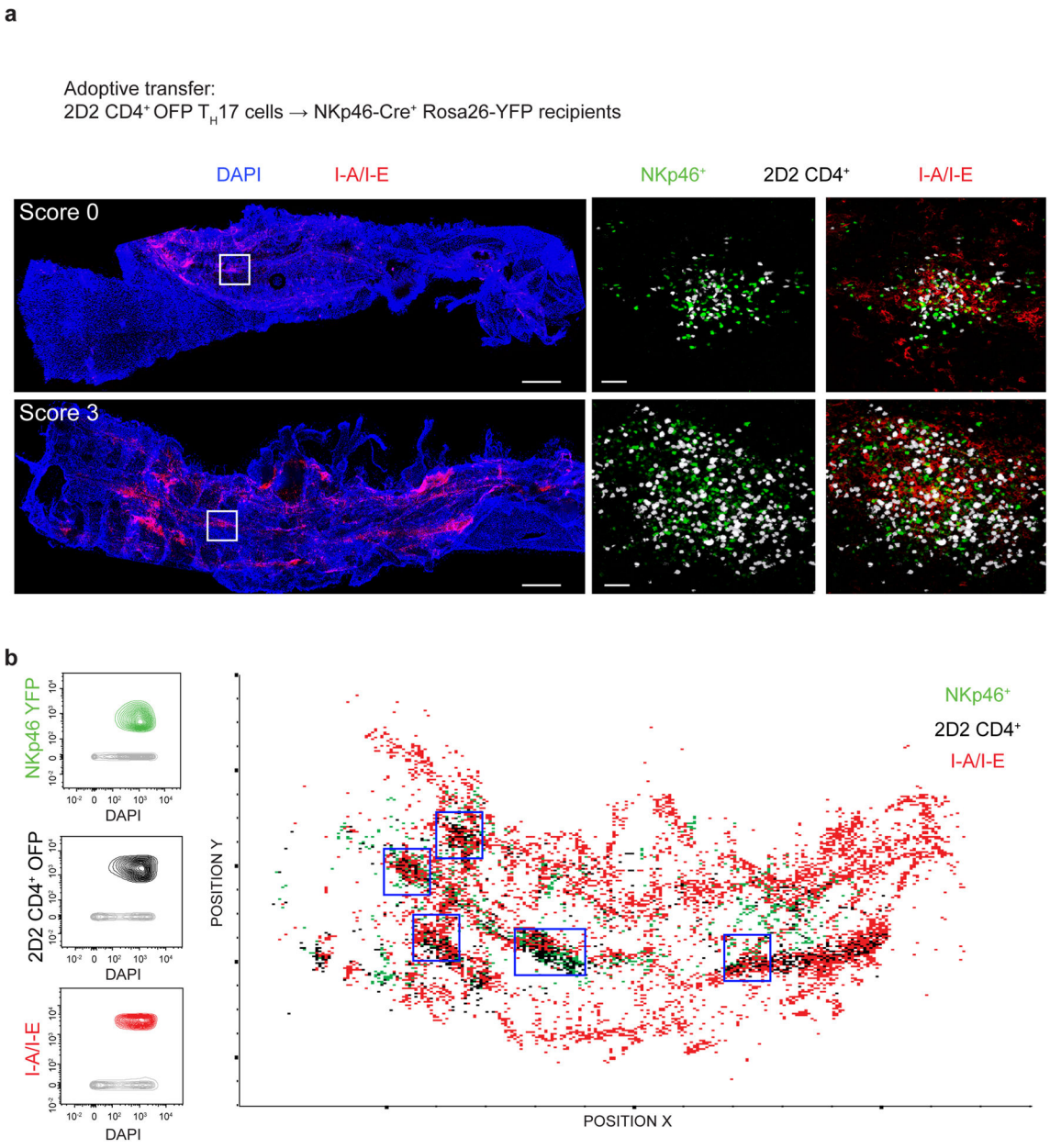

Figure 5.

Localization of T-bet-dependent NKp46^{+} ILCs during EAE. (**a**) A total of 7.5 × 10^{6} 2D2 CD4^{+} OFP^{+} T_H17 cells were adoptively transferred into NKp46^{+} reporter mice (NKp46-Cre^{+} *Rosa26-lox*P-STOP-*lox*P-YFP). Spinal cord meninges were isolated from NKp46^{+} reporter mice before the onset of symptoms (score 0) and during the peak of disease (score 3) and stained with DAPI and anti-MHCII (I-A/I-E). Inset images show clusters of NKp46^{+} (green) and 2D2 CD4^{+} T cells (white), without (left) and with (right) MHCII (I-A/I-E) staining. Scale bars, 500 mm for main images or 40 µm for insets. (**b**) Spots statistics from the whole mount shown in (**a**) (score 3) were exported and plotted for identification of distinct immune subsets. NKp46-YFP^{+}, 2D2 CD4^{+} OFP and I-A/I-E voxel gating allowed identification and spatial visualization of the NKp46^{+} ILCs, 2D2 CD4^{+} T cells and MHCII-

expressing APCs, respectively, by histo-cytometry (as described in **Methods**). Histological analysis is representative of 2 independent experiments (n = 3 mice for score 0 and n = 4 mice for score 3).

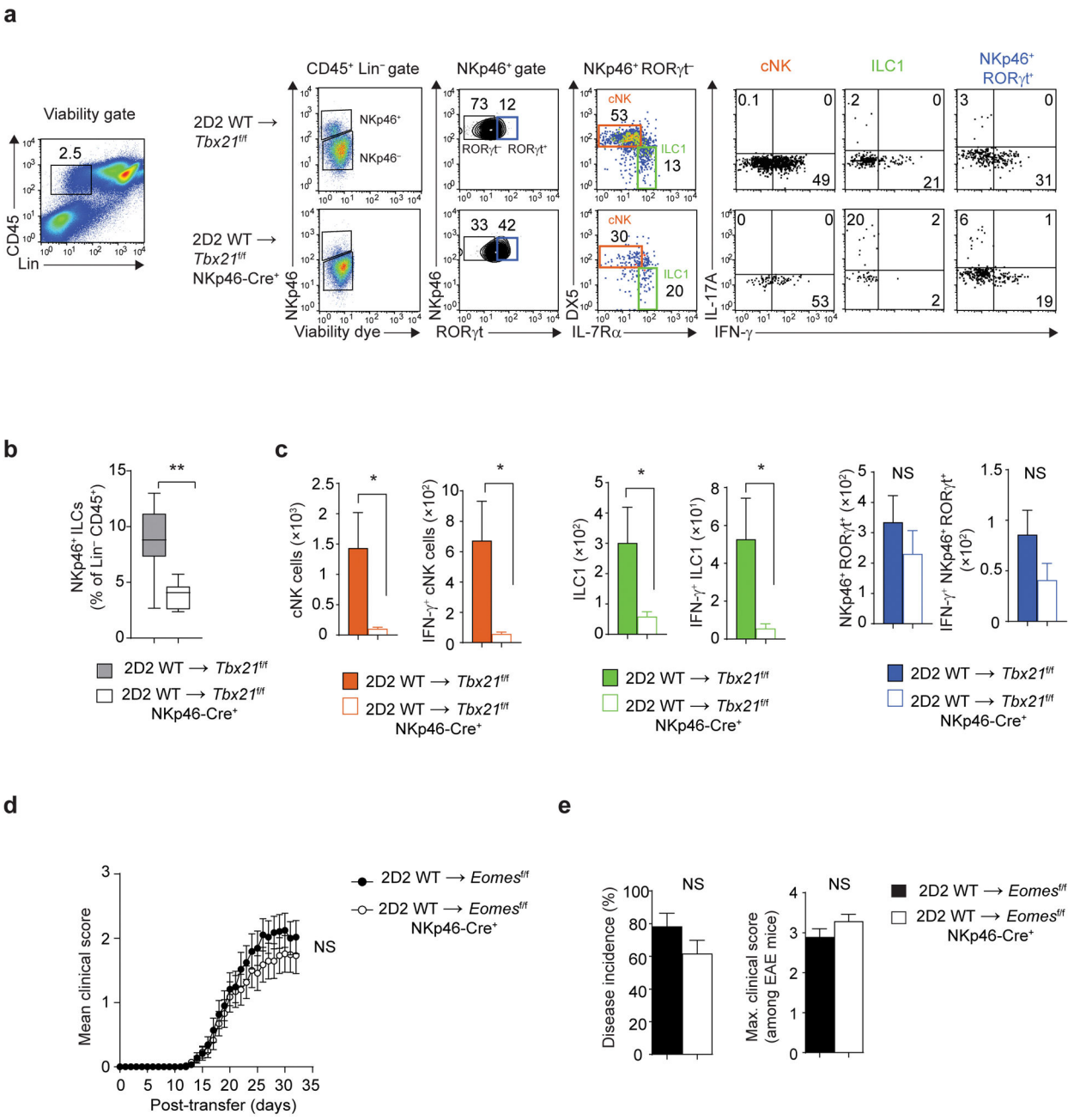

Figure 6.

Pathogenic function of T-bet maps to ILC1/NKp46$^+$ ILC3. (**a**) Flow cytometry analysis of meningeal immune cells following adoptive transfer of 7.5 × 10^6 2D2 WT T_H17 cells into *Tbx21*$^{f/f}$ or *Tbx21*$^{f/f}$ NKp46-Cre$^+$ mice. Cells were stimulated with PMA and ionomycin for 3 h in the presence of monensin in the last 1.5 h of stimulation. Stimulated cells were stained with viability dye, antibodies to lineage markers (TCRβ, TCRγδ, B220, Gr1) and anti-CD45, anti-NKp46, anti-IL-7Rα, anti-CD49b (DX5), anti-RORγt, anti-IL-17A and anti-IFN-γ. Production of IL-17A and IFN-γ by meningeal NK cells (gated on Lin$^-$CD45$^+$NKp46$^+$RORγt$^-$DX5$^+$IL-7Rα$^-$), ILC1 (gated on

$Lin^{-}CD45^{+}NKp46^{+}ROR\gamma t^{-}DX5^{-/lo}IL\text{-}7R\alpha^{+}$) and $NKp46^{+}$ ILC3 (gated on $Lin^{-}CD45^{+}NKp46^{+}ROR\gamma t^{+}IL\text{-}7R\alpha^{+}$) was measured by intracellular cytokine staining. (**b**) The box-and-whiskers plot depict the frequency of $NKp46^{+}$ ILCs within $Lin^{-}CD45^{+}$ population in the meninges of *Tbx21*$^{f/f}$ or *Tbx21*$^{f/f}$ NKp46-Cre^{+} mice. (**c**) Absolute numbers of NK cells, ILC1 and $NKp46^{+}$ ILC3 and IFN-γ-producing NK cells, ILC1 and $NKp46^{+}$ ILC3 (gated as in **a**) in the meninges of *Tbx21*$^{f/f}$ or *Tbx21*$^{f/f}$ NKp46-Cre^{+} mice. (**d–e**) Mean clinical scores, percent disease incidence and maximum clinical score of *Eomes*$^{f/f}$ or *Eomes*$^{f/f}$ NKp46-Cre^{+}mice following adoptive transfer of 7.5×10^{6} 2D2 WT T_H17 cells. NS, $P > 0.05$; *, $P < 0.05$; **, $P < 0.001$ (two-tailed Student's *t*-test (**b**,**c**,**e**) or two-way ANOVA (**d**)). Data are combined from two independent experiments (**b**,**c**; $n = 9$, 10 mice per group) or three independent experiments (**d**,**e**; $n = 29$, 35 mice per group).

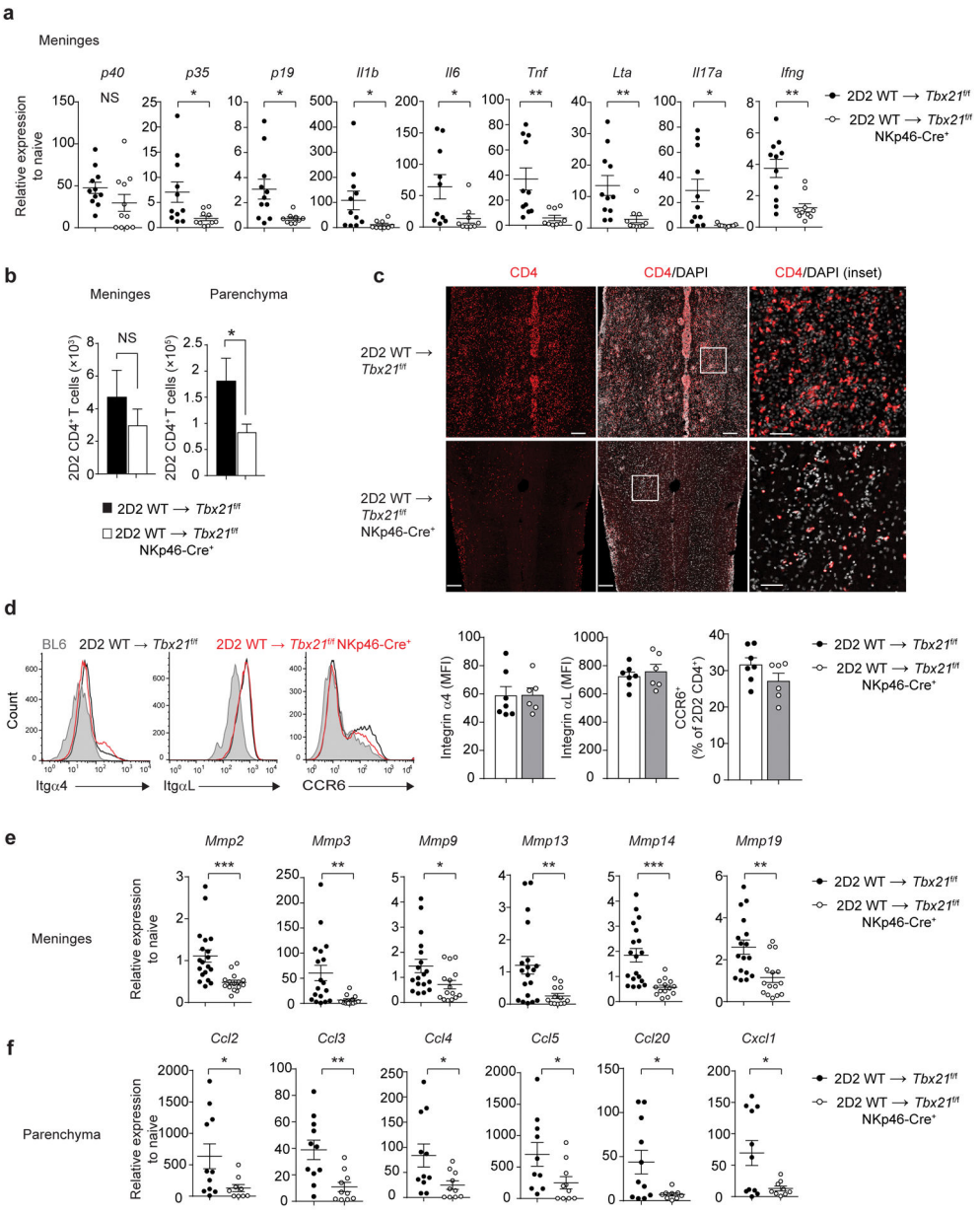

Figure 7.

NKp46^{+} ILCs regulate infiltration of CD4^{+} T_H17 cells. (**a**) Quantitative RT-PCR analysis of genes encoding pro-inflammatory cytokines in the spinal cord meninges of *Tbx21*$^{f/f}$ or *Tbx21*$^{f/f}$ NKp46-Cre^{+} mice following the adoptive transfer of 7.5 × 10^{6} 2D2 WT T_H17 cells. Gene expression is presented relative to the housekeeping gene *Hprt*, and normalized to transcript abundance from naïve WT (BL6) mice. (**b**) Absolute number of 2D2 CD4^{+} T cells (CD4^{+}V$_{\beta}$11^{+}) in the spinal cord meninges and CNS parenchyma of *Tbx21*$^{f/f}$ or *Tbx21*$^{f/f}$ NKp46-Cre^{+} mice as quantitated by flow cytometry. (**c**) Immunohistological analysis of longitudinal spinal cord sections from *Tbx21*$^{f/f}$ or *Tbx21*$^{f/f}$ NKp46-Cre^{+} mice following the adoptive transfer of 2D2 WT T_H17 cells. Tissue sections were stained with DAPI and anti-CD4. Scale bars, 200 μm for main images or 50 μm for insets. (**d**) Expression of integrins

α_4, α_L and CCR6 on CNS-infiltrating 2D2 $CD4^+$ T cells (day 18–20 post-adoptive transfer). Bar graphs depict the average mean fluorescence intensity (MFI) of α4 and αL staining and mean percentage of $CCR6^+$ 2D2 $CD4^+$ T cells. (**e–f**) Quantitative RT-PCR analysis of genes encoding matrix metalloproteinases (MMPs) in the spinal cord meninges and chemokines in the spinal cord parenchyma of *Tbx21*$^{f/f}$ or *Tbx21*$^{f/f}$ NKp46-Cre^+ mice (quantified as in **a**). *, $P < 0.05$; **, $P < 0.01$; ***, $P < 0.001$ (two-tailed Student's *t*-test). Data are combined from two independent experiments (**a**,**f**; mean ± s.e.m. of $n = 11$ mice per group, **d**; $n = 6$, 7 mice per group), three independent experiments (**e**; mean ± s.e.m. of $n = 15$, 19 mice per group) or four independent experiments (**b**; mean ± s.e.m. of 17 mice per group). Histology images are representative of 2 independent experiments ($n = 6$ mice per group).

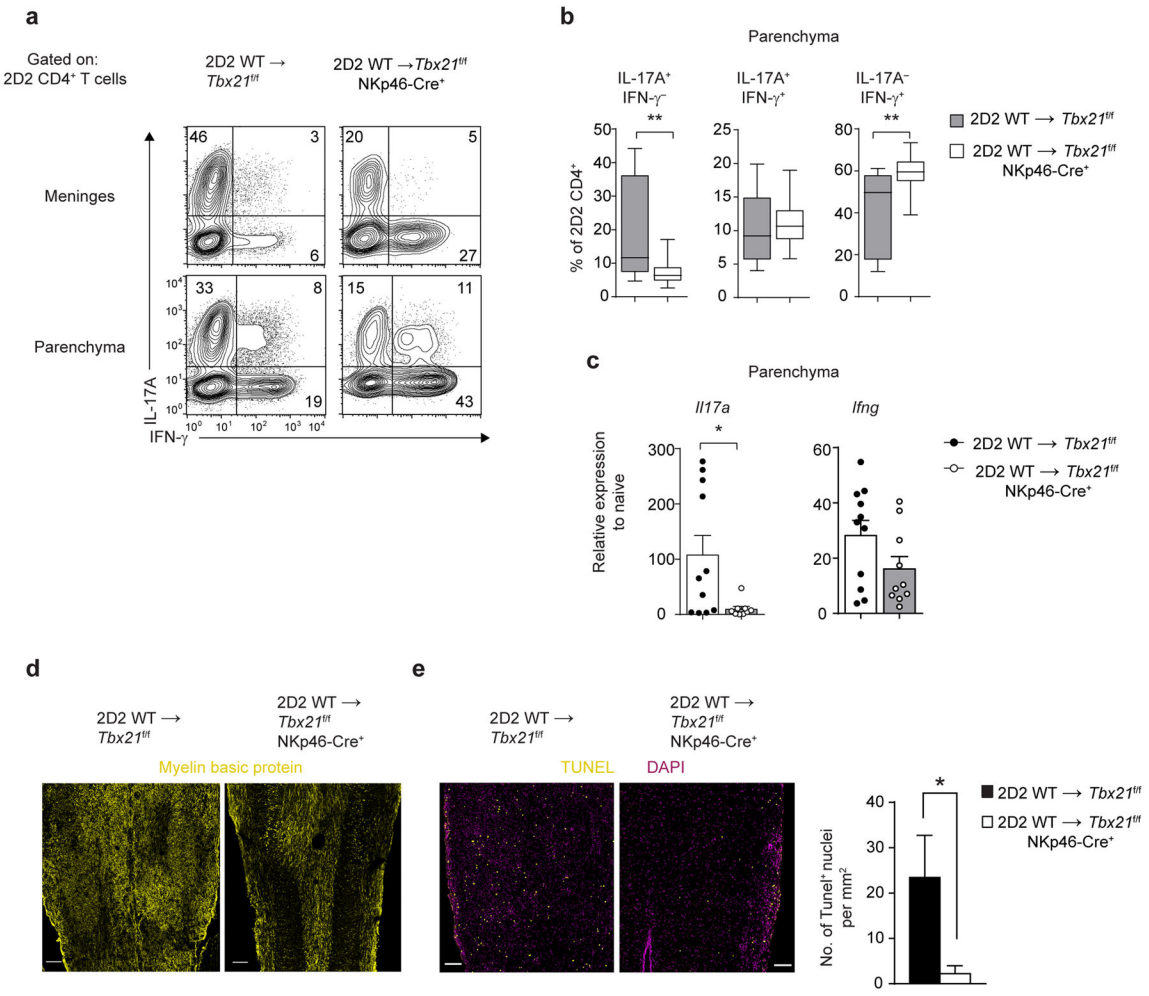

Figure 8.

NKp46$^+$ ILCs regulate the stability of CD4$^+$ T_H17 cells. (**a**) Intracellular cytokine staining of 2D2 CD4$^+$ T cells isolated from the meninges and CNS parenchyma of *Tbx21*$^{f/f}$ or *Tbx21*$^{f/f}$ NKp46-Cre$^+$ mice following adoptive transfer of 7.5 × 10^6 2D2 WT T_H17 cells. (**b**) Box-and-whiskers plots of cytokine producing 2D2 CD4$^+$ T cells isolated from the CNS parenchyma of *Tbx21*$^{f/f}$ or *Tbx21*$^{f/f}$ NKp46-Cre$^+$ mice. (**c**) Quantitative RT-PCR analysis of genes encoding IL-17A and IFN-**γ** in the CNS parenchyma of *Tbx21*$^{f/f}$ or *Tbx21*$^{f/f}$ NKp46-Cre$^+$ mice (quantified as in Fig. 7a). (**d–e**) Longitudinal spinal cord sections from *Tbx21*$^{f/f}$ or *Tbx21*$^{f/f}$ NKp46-Cre$^+$ mice were stained with anti-myelin basic protein antibody. TUNEL staining was performed to quantitate apoptotic cell death in the spinal cord tissue, and results were normalized to the total tissue area analyzed. Scale bars, 200 μm (**d**) or 100 μm (**e**). ***, *P < 0.05*; **, *P < 0.001* (two-tailed Student's *t*-test). Data are representative of 2 independent experiments (meninges) or five independent experiments (parenchyma) (**a**), or combined from five independent experiments (**b**; *n* = 24, 28 mice per group) and 2 independent experiments (**c;** *n* = 10, 11 mice per group). Histology images are representative of 2

independent experiments, while TUNEL analysis was performed on 2 sections per mouse, with 3–4 mice per group (**d–e**).